Eur. Phys. J. B **35**, 301–309 (2003)
DOI: 10.1140/epjb/e2003-00281-5

THE EUROPEAN PHYSICAL JOURNAL B

The high-pressure phase sequence in nanocrystalline zirconia

P. Bouvier[a], V. Dmitriev, and G. Lucazeau

Laboratoire d'Électrochimie et de Physico-Chimie des Matériaux et des Interfaces, INPG-CNRS, 1130 rue de la Piscine, BP 75, 38402 St. Martin d'Hères Cedex, France

Received 31 January 2003 / Received in final form 29 July 2003
Published online 15 October 2003 –

Abstract. X-ray diffraction and Raman data on the pressure induced phase transitions of a nanometric zirconia, ZrO_2, are analyzed *via* a classical phenomenological Landau approach of the bulk. It is concluded that the initial tetragonal structure (D_{4h}^{15}), which is a metastable bulk state of zirconia at ambient conditions, evolves continuously towards the ideal cubic fluorite structure (O_h^5) *via* an intermediate tetragonal form (D_{4h}^{14}). The proposed phenomenological model describes consistently all experimental peculiarities, including the hybridization and softening of the low-frequency Raman active modes along with lattice-parameter anomalies.

PACS. 64.70.Nd Structural transitions in nanoscale materials – 61.50.Ks Crystallographic aspects of phase transformations; pressure effects – 61.10.Nz X-ray diffraction

1 Introduction

Although zirconia, ZrO_2, was and remains a subject of intensive studies and practical importance, its theoretical description is characterized by controversial results. Atomistic mechanisms for the phase transitions seem to be clear owing to reliable structural information. However, the driving forces behind the transformations and their detailed mechanisms are still not understood. The understanding of the detailed atomistic scheme of phase transitions, that occurs at ambient pressure from the high-temperature cubic (**c**) fluorite-type (O_h^5, $Fm3m$, Z=1), to the tetragonal (**t**) (D_{4h}^{15}, $P4_2/$nmc, Z=2) and then to the monoclinic (**m**) (C_{2h}^5, $P2_1/c$, Z=4) has stimulated theoretical work over the last decades. A group theory analysis showed that both the **c-t** and **t-m** transitions may be induced by condensation of modes belonging to special points of the Brillouin zone (BZ) [1–3], namely the X point of the parent cubic BZ. The soft mode driven mechanism received support from lattice-dynamical calculations [4,5] and was further confirmed by *ab initio* calculations, from which an imaginary phonon frequency for the particular X_2^- non-degenerate mode was obtained [6–11].

New studies were prompted by the synthesis of nanosized zirconia. A supplementary parameter, the particle size, which changes the stability conditions for the phases, came into consideration. Recent high-pressure experiments performed on pure nanometric tetragonal ZrO_2 [12,13] have shown that the tetragonal structure, at variance with the compressed microcrystalline phase sequence **m**($P2_1/c$)-OI($Pbca$)-OII($Pnam$), evolves continuously toward the ideal fluorite **c**($Fm3m$) structure. The authors arrived at this conclusion through the observation of the ratio c/a of the crystallographic parameters which evolves continuously towards unity together with the six Raman bands of the initial spectrum. Upon extrapolation to 40 GPa, these tend toward a single band as expected in the fluorite phase [12,13]. Although the transition pressure was not reached in the Raman experiment, the extrapolation of the evolution of the spectral parameters provided the same transition pressure as found in the X-ray experiment. In addition, a "spectacular" softening of the 260 cm^{-1} Raman active mode was observed. It was tempting to invoke the classical scenario of cell doubling induced by condensation of the X_2^- phonon at the cubic BZ boundary.

However, a strong interaction of the 260 cm^{-1} soft mode with a 150 cm^{-1} low frequency mode was found. The corresponding repulsion (hybridization) of the modes becomes observable above 8 GPa and reaches a maximum at 20 GPa. Anharmonic processes allowing the mixing of fundamental modes of different symmetry or overtones (*e.g.* Fermi resonance) were rejected as possible explanation because they do not account for the strong coupling and the initial intensity of both modes. These observations have led the authors to conclude that the two modes are of the same symmetry and could not belong to the A_{1g} representation of the D_{4h}^{15} initial phase. Two possibilities are then offered. Either these modes are of E_g symmetry (as proposed in Ref. [14]), or an intermediate phase exists in which two modes of the same symmetry could drive the

[a] e-mail: Pierre.Bouvier@lepmi.inpg.fr

transition towards the O_h^5 space-group. The possibility of the latter was reinforced by the observation of a sudden decrease of the c/a ratio at about 8 GPa, the pressure near which the repulsion becomes measurable [12].

The present study intends to clarify the situation. To this effect, new high-resolution X-ray diffraction and Raman data were analyzed along with earlier data, taking into account the possible structural changes. The paper is organized as follows. In the first part, results of high-pressure X-ray diffraction are presented. The second part is devoted to a phenomenological analysis of the phase symmetry and transition mechanisms in bulk ZrO_2. It is shown that the combination of experimental results, such as the c/a evolution and the observation of interacting soft modes, along with a group-theory analysis provide a single possible mechanism and confirms the fluorite structure of the high-pressure phase.

2 Experimental results

2.1 Methods

High-pressure synchrotron X-ray diffraction (XRD) experiments were performed at the European Synchrotron Radiation Facility (ESRF, Grenoble, France) on the ID30 beam line. The sample was loaded in a diamond anvil cell with diamond culets of 350 μm diameter. Nitrogen was used as pressure transmitting medium to keep quasi-hydrostatic conditions over a wide pressure range. The pressure was measured using the ruby fluorescence method with a precision of 0.1 GPa below 20 GPa [15]. X-ray diffraction patterns were collected in angle-resolved geometry on an image-plate detector (Mar345) with a focused monochromatic beam at wavelength $\lambda = 0.3738(1)$ Å. The sample-to-detector distance and the image-plate inclination angles were precisely calibrated using a silicon standard. The two-dimensional diffraction images were analyzed using the ESRF Fit2D software, yielding intensity *vs.* 2θ patterns [16]. The patterns were analyzed by least-square refinement of both (110) and (002) reflections located respectively at $2\theta = 8.29°$ and 8.45° using pseudo-Voigt peak-shape functions.

Undoped tetragonal zirconia was prepared by spray pyrolysis using an ultrasonic atomizer [17]. This technique gives nanocrystallized material with the tetragonal structure stable at room temperature. The average crystallite size was 18±2 nm based on the Scherrer equation. The monoclinic zirconia content was below 1 wt% both from Raman spectrometry and quantitative X-ray diffraction measurements [18].

2.2 X-ray diffraction: results and discussions

X-ray diffraction patterns of the nanometric zirconia samples recorded between 1.0 and 18.4 GPa are presented in Figure 1. All diagrams were perfectly fitted with a tetragonal lattice in full agreement with the previous study [13], however the pressure dependence of the tetragonal cell

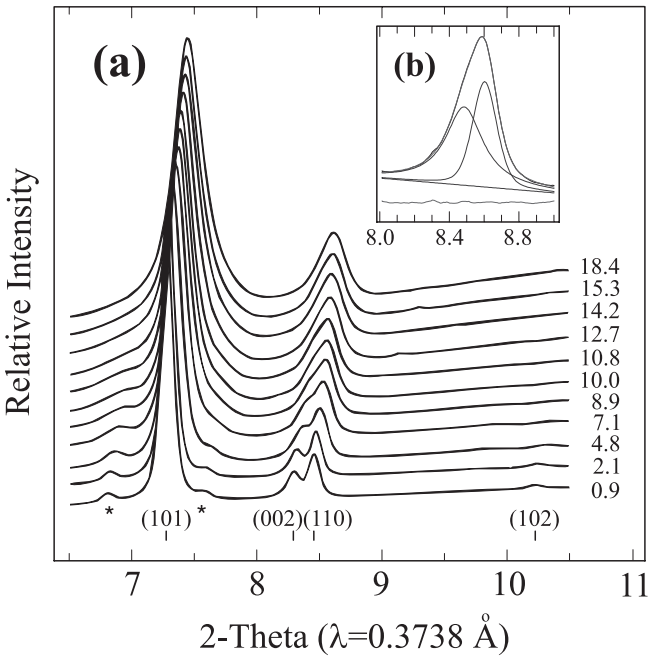

Fig. 1. (a) X-ray diffraction patterns of undoped tetragonal zirconia (18 nm) with increasing pressure between 1 and 18.4 GPa. The tick marks represent the expected lines for the tetragonal D_{4h}^{15} cell. The weak reflections, which are observed at $2\theta = 6.80$ and 7.57 degrees and are indicated by stars, are due to a small proportion of the monoclinic phase (C_{2h}^5). This contribution does not evolve with pressure. Notice that the splitting of the doublet (002)-(110) demonstrates that the tetragonal distortion persists up to 18 GPa (b).

parameters, drawn in Figure 2, differs considerably from the one published earlier. The present resolution is much better than in reference [13] and allows to observe separately the (002)-(110) lines between 1 and 12 GPa. No new satellite peaks corresponding to a new superstructure were found. In the 12–20 GPa pressure range, it is still possible to reproduce the experimental peak by two pseudo-Voigt components. At variance with published data, the present data indicate that the c and a lattice parameters are still different at 20 GPa. The clear discontinuity of the c/a ratio at about 8 GPa deduced from the previous study [13] is not confirmed. Actually, because these lines were not clearly resolved in the previous study, this conclusion was based on Rietveld refinements of diagrams as a whole. By extrapolation of the c and a plots to high-pressure (Fig. 2), one may see that the cubic structure is reached at about 40 GPa.

The pressure dependence of the cell volume is satisfactorily reproduced by a second-order Birch-Murnaghan equation of state with parameters $V_0 = 66.84(8)$ Å^3, $K_T = 170(10)$ GPa and $K' = 4.3(1.3)$ in good agreement with the previous study [13]. However, in Figure 2, a linear extrapolation of the experimental plots below 10 GPa shows that c and a become equal to 3.4 Å for $P \simeq 36$ GPa. This value is different from the 40 GPa found from extrapolation in the 10–40 GPa range. The

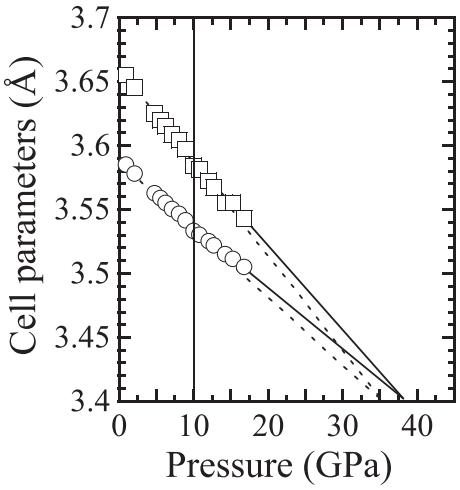

Fig. 2. Evolution with pressure of the cell parameters in tetragonal zirconia obtained from least-square refinement of the (200)-(110) doublet. The pressure dependence of the volume is described by a third order Birch-Murnaghan equation of state with parameters given in the text. Dashed and plain lines correspond to linear extrapolation in the low ($P < 10$ GPa) and high ($10 < P < 40$ GPa) pressure range respectively.

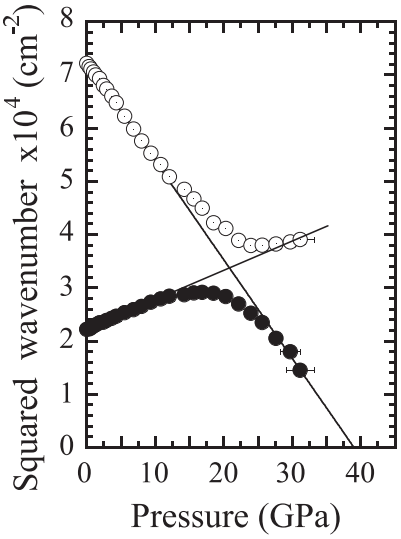

Fig. 3. Evolution with pressure of the squared wavenumber ω^2 of the two lowest Raman modes initially located at 150 and 260 cm^{-1}. Straight lines are the best least-square fits.

existence of two different compressibilities suggests a structural change. The use of a linear extrapolation of the experimental data rather than a fit to an equation of state is in line with a Landau-type phenomenological theory. This will be discussed below. Thus, as a preliminary conclusion of the X-ray study, a discontinuity in the derivatives of the lattice-parameters pressure plots suggests that the sample undergoes a structural change at 10 GPa accompanied by a small anomaly.

2.3 High-pressure phase transitions

2.3.1 Displacive character for the transition near 40 GPa

In our previous experiment [12] we found a soft-mode behavior of the Raman active vibration $\omega_{sm} = 260$ cm^{-1} shown in Figure 3. The observation of such a well-pronounced soft mode in the vibrational spectra of ZrO_2 strongly suggests that the transition at ∼40 GPa is displacive. This is in agreement with the continuous evolution of the different spectral parameters, and all these experimental facts are in favor of a second-order transition near 40 GPa. The pressure dependence of the hybridized soft mode (Fig. 3) obeys a law $\omega^2 = \alpha(1\text{-}P/P_0)^\beta$, with $\beta = 0.945$ and $P_0 = 38.03$ GPa. The exponent β nearly equals unity like in a pure displacive second-order phase transition. The displacive mechanism is more evident for the *pressure-induced* transformation than for the *temperature-induced* cubic O_h^5 to tetragonal D_{4h}^{15} transition taking place at 2300 °C in the microcrystalline and single-crystalline pure zirconia. The interpretation of these experimental data regarding the mechanism of the latter transition has been very controversial. In particular, no direct observation of a soft mode is reported in the literature. However this transition can be interpreted in terms of Landau theory, and the "condensation" of the phonon mode is believed to be at the origin of the tetragonal distortion by antiparallel displacements of oxygen atoms along the z-axis [1–11]. In this process, the mode X_2^- becomes the *unique* zone centre A_{1g} mode of the low symmetry tetragonal D_{4h}^{15} daughter-phase. Several lattice-dynamical and *ab initio* calculations [4,5,7–11,19] have found that the X_2^- mode of the cubic phase indeed becomes unstable close to the transition temperature, supporting the above scheme.

The experimental observation of anticrossing is a clear proof that the two interacting modes are of the same symmetry. Thus, they cannot be of A_{1g} symmetry as there is only one A_{1g} mode in the Raman spectrum of tetragonal zirconia [20]. Consequently, the above temperature-controlled scenario is not appropriate for the pressure induced tetragonal-cubic transition and it should be complemented by a new transformation mechanism. This conclusion again brings our attention to the possible transition at 10 GPa discussed above.

2.3.2 Experimental evidence for the existence of an intermediate phase in the 8–40 GPa range

In the pressure evolution of the Raman spectra, it is worth noting that there is an evident anomaly observed near $P = 10$ GPa, as already mentioned in reference [12]. The signature of this anomaly is a change of slope in the pressure dependence of the mode frequencies (see Fig. 3 of Ref. [12]). An identical anomaly is found in experiments employing different pressure transmitting media (an alcohol mixture in Raman experiments contra nitrogen in the XRD one), giving it more weight.

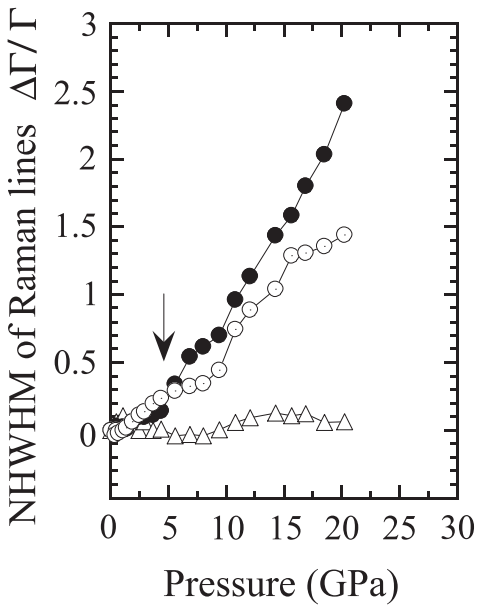

Fig. 4. Normalized Half-Width at Half-Maximum (*NHWHM*), $\left(\Gamma^P - \Gamma^P_{n-h}\right)/\Gamma^{P=0}$, corrected from the expected *HWHM*, Γ_{n-h}, owing to pressure non-hydrostaticity which was measured from the broadening of the R_1 ruby luminescence line (see text). The open triangles display the behavior of the 639 cm^{-1} mode, open circles: $\omega = 260$ cm^{-1}, solid circles: $\omega = 150$ cm^{-1}.

Another important effect is the interaction of the low-frequency modes. As already stated above, the repulsion (hybridization) of the two low-frequency modes (which implies a deviation of the corresponding pressure dependence from linear) begins to be observable from 8 GPa and continues up to 20 GPa. This interaction seems to begin even sooner as seen from the Normalized Half Width at Half-Maximum *(NHWHM)* in Figure 4. The Normalized half-width at half-maximum $NHWHM^P = \left(\Gamma^P - \Gamma^P_{n-h}\right)/\Gamma^{P=0}$ is obtained at each pressure P using the half-width at half-maximum *(HWHM)* of Raman bands, Γ^P and $\Gamma^{P=0}$ measured at pressure P and at atmospheric pressure respectively. Both are directly measured from the Raman spectrum. The non-hydrostatic contribution of the broadening, Γ^P_{n-h}, defined as $\Gamma^P_{n-h} = \Gamma^{P=0} + \beta\sigma^P$, is calculated at each pressure P using the slope β of the linear pressure dependence of Raman bands wavenumber, (in $cm^{-1}.GPa^{-1}$ see Ref. [12]). This slope is measured in the low pressure range where pressure is known to be hydrostatic. The coefficient σ^P, defined as $\sigma^P = (1/\alpha)(\Gamma^P_{R1} - \Gamma^{P=0}_{R1})$, is obtained using, the *HWHM* of the R1 ruby line, Γ^P_{R1} and $\Gamma^{P=0}_{R1}$, measured at pressure, P, and at atmospheric pressure and the slope α of the linear pressure dependence of the R1 ruby line wavenumber. It is clearly seen, in Figure 4, that the 150 cm^{-1} and 260 cm^{-1} modes undergo an anomalous broadening from 5 GPa upward while another non-interacting high-frequency 639 cm^{-1} mode keeps its *HWHM* constant. It is worth noting that the same applies to all high-frequency modes. Therefore the anomalies are intrinsic and the observed effects cannot be attributed to any non-hydrostatic stresses arising from a stiffening of the pressure transmitting medium, or to energy separation when probing the phonon density of states.

3 Penomenological models

3.1 High-pressure cubic phase

The complete set of Raman scattering and X-ray diffraction data allows to check in detail possible phase transitions in nanometric zirconia. However, first we will summarize the results of a symmetry analysis of isobaric transformations in the microcrystalline ZrO_2 published earlier [1–3].

In its high-temperature parent phase, ZrO_2 belongs to the fluorite-structure type (space group O^5_h, $Z = 1$). Zirconium cations occupies the one-fold position (a): (0, 0, 0), while oxygens anions are located in the two-fold position (c): (0.25, 0.25, 0.25). The second-order phase transition at T_1=2300 °C and ambient pressure, lowering the symmetry from cubic to tetragonal (D^{15}_{4h}, $Z = 2$), is induced by an instability of the cubic structure with respect to the X^-_2 phonon displacements at the X=[0, 0, $2\pi/a$] point of the Brillouin zone (BZ) boundary. The next transition takes place at T_2=900 °C, and leads to the monoclinic baddeleite-type phase (C^5_{2h}, $Z = 4$). This transition is caused by an *additional* instability at the same BZ point X but with respect to another critical phonon, X^-_5. Both transition mechanisms include macroscopic deformations of the parent unit cell: tetragonal (uniaxial tensile) and monoclinic (tensile, stretch and shear) correspondingly.

In terms of the Landau phenomenological theory these transitions are *improper ferroelastic* transitions of the fluorite cubic parent-phase. In such transitions, the second-rank strain-tensor components play the role of secondary order parameters (OPs) induced by the primary displacive instabilities at the X-point of the fcc BZ. The corresponding primary OP components are either the three-dimensional irreducible representation (IR) X^-_2 or the six-dimensional IR X^-_5 of the O^5_h parent-phase space group. The structure distortion in the tetragonal phase can be characterized by a single non-zero X^-_2 OP component, while the transformation into the monoclinic phase needs *in addition* two (out of six) non-zero components of the X^-_5 OP.

In nanometric zirconia, first, we find in the high-pressure phases no superstructure (new translational symmetry) different from known ones. This allows us to restrict a search for possible OPs to the X point of the BZ boundary. Second, the occupancy of structural positions in different phases of ZrO_2, and the absence of any kinetic indications of disordering (or reordering) processes reasonably allows to consider the high-pressure transformations in nanocrystalline ZrO_2 as displacive ones. Lastly, one can conclude that the absence of discontinuities in the pressure dependencies of various physical parameters

Table 1. Low-symmetry tetragonal and cubic phases associated with displacive transitions at the X point of fcc BZ (three-dimensional IRs). $\Delta\rho$ is an equilibrium relationship between order-parameter components. n is the phase label used in Figure 5.

n	$\Delta\rho$	X_1^+	X_2^-	X_4^-	Z
1	$\delta_1 = \delta_2 \neq 0, \delta_3 = 0$	-	D_{4h}^3	D_{4h}^{10}	4
2	$\delta_1 \neq 0, \delta_2 = \delta_3 = 0$	D_{4h}^1	D_{4h}^{15}	D_{4h}^7	2
3	$\delta_1 = \delta_2 = \delta_3 \neq 0$	O_h^1	T_d^1	T_d^1	4

Table 2. Low-symmetry tetragonal and cubic phases associated with displacive transitions at the X point of the fcc BZ (six-dimensional IRs).

n	$\Delta\rho$	X_5^+	X_5^-	Z
1	$-\delta_3 = \delta_6 \neq 0, \delta_i = 0$	D_{4h}^5	D_{4h}^7	4
2	$\delta_4 = \delta_5 \neq 0, \delta_i = 0$	D_{4h}^{16}	D_{4h}^{14}	4
3	$\delta_1 = \delta_2 = \delta_3 \neq 0, \delta_i = 0$	T_h^6	T^4	4

indicates a continuous onset of only slight distortions in the structure. However, the large difference in the atomic form factors for zirconium and oxygen makes it non-trivial to observe small distortions in the oxygen sublattice. For the sake of generality, we consider the high-pressure phase ($P > 40$ GPa) as being cubic but do not assign it *a priori* to the parent fluorite-type structure.

The reducible representation in the ZrO_2 structure at the Γ and X points of the BZ, constructed on the (a) and (c) positions of the O_h^5 space group, can be reduced into IRs as follows:

$$\mathbf{M}(ZrO_2) = \left[F_{1u} + X_4^- + X_5^-\right]_{Zr} + \left[F_{1u} + F_{2g} + X_1^+ + X_2^- + X_5^+ + X_5^-\right]_O. \quad (1)$$

Among the IRs $X_i^\pm$ one should find OPs that describe the pressure-induced displacive phase transformations of nanocrystalline zirconia. The continuous character of the corresponding transitions allows to consider these transitions, not only in the framework of the model-free *symmetry* part of the phenomenological theory, but to extend our consideration to its *thermodynamic* part based on the series expansion of a variational free energy.

Tables 1 and 2 give the list of tetragonal and cubic distorted phases associated with the displacive mechanisms involving phonons appearing in equation (1), obtained by using the formalism of image (matrix) groups. This list, containing only thermodynamically stable phases but not restricted to subgroups of the parent-phase space group, is the result of a model-free geometrical consideration in OP space (see, *e.g.* [21,22]). Hence, it is complete and exhausts all possible distorted tetragonal and cubic structures. Tables 1 and 2 are supplemented with equilibrium relations between OP components δ_{ij}, which characterize a contribution of each symmetry coordinate (linear symmetrical combination of atomic shifts) in the total structure distortion:

$$\Delta\rho(x,y,z) = \sum_{i,j} \delta_{ij}\varphi_{ij}(x,y,z). \quad (2)$$

Here, $\Delta\rho$ is the increment of probability density in a crystal at a phase transition and $\varphi_{ij}(x,y,z)$ is the ith basis function of IRs labeled by index j.

Two candidates from (1) - X_1^+ and X_5^+, violate the Landau condition, because the corresponding variational free energy expansions in the OP components (the Landau potentials) contain cubic terms [23], and therefore a second-order phase transition is possible only at an isolated point of the phase diagram. Thus, neither continuous variation of measurable parameters nor the soft-mode behavior, observed experimentally in nanometric ZrO_2, can be described in the framework of the corresponding models.

Two other OPs, X_2^- and X_4^-, belong to the same matrix group (group of matrices of IR) that is isomorphous to point group O_h. The integrity basis of invariants associated with the matrix group O_h is

$$\begin{aligned} I_1 &= \delta_1^2 + \delta_2^2 + \delta_3^2, \\ I_2 &= \delta_1^4 + \delta_2^4 + \delta_3^4, \\ I_3 &= \delta_1^2\delta_2^2\delta_3^2. \end{aligned} \quad (3)$$

The simplest sixth degree expansion written below is sufficient to describe the main features of the transitions between the phases listed in Tables 1 and 2:

$$F(I_1, I_2, I_3) = a_1 I_1 + a_2 I_1^2 + b_1 I_2 + c_1 I_3 + d_{12} I_1 I_2. \quad (4)$$

The potential of equation (4) was first introduced in reference [24] for describing the structural phase transitions in $BaTiO_3$. A generalized phase diagram of the corresponding thermodynamic system was studied comprehensively in references [21,25] (see also a review in [22]), and these results are used in the present work without going into details. Figure 5 shows a section of a generalized phase diagram of the O_h matrix group. This diagram, mapped on the $(a_1 - b_1)$ coordinate plane of the expansion coefficients, contains all phases of interest. At first glance, the X_2^- OP (Tab. 1, Fig. 5) provides a possibility for an adequate theoretical description since, in accordance with expectations, it induces, with decreasing temperature, a second-order phase transition from the fluorite cubic phase $O_h^5(1)$ (phase 0) to the tetragonal $D_{4h}^{15}(2)$ (phase 2) and then two consecutive pressure-induced phase transitions to tetragonal $D_{4h}^3(4)$ (phase 1) and cubic $T_d^1(4)$ (phase 3) phases (Fig. 5). At least on the level of point groups, such predicted behavior satisfies our starting criteria. However, the existence of a well-pronounced softening of a low-frequency vibrational mode observed in the Raman spectra of ZrO_2 (Fig. 3) contradicts some of these theoretical predictions. First, because the centrosymmetric tetragonal D_{4h}^3 phase and non-centrosymmetric cubic T_d^1 are not connected by a "group-subgroup" relationship, there is no reason to expect the observation of a soft mode. Second, for

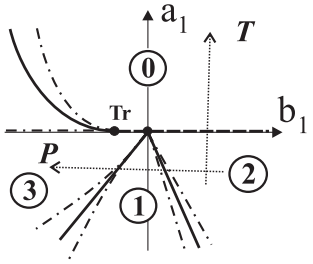

Fig. 5. Phase diagram corresponding to the matrix group O_h. Full, dashed, and dash-dotted lines are first-order, second-order and limit of stability lines, respectively. Tr is a tricritical point. Dotted lines show possible P-T axis positions. Numbers in circles correspond to the phases in Table 1.

Table 3. Correlation of irreducible representations of the O_h^5 space group in different low-symmetry phases.

$O_h^5(1)$	$D_{4h}^{15}(2)$	$D_{4h}^{14}(4)$	$D_{4h}^{7}(4)$
X_1^+	B_{2u}	$B_{2g}+E_u$	$A_{1g}+A_{2u}+B_{2u}$
X_2^-	A_{1g}	$A_{2u}+E_g$	$A_{2g}+B_{1u}+B_{2g}$
X_4^-	B_{1g}	$A_{2g}+B_{2g}+B_{1u}$	$A_{1u}+E_g$
X_5^+	E_u	$A_{1u}+B_{1u}+E_g+E_u$	$A_{1g}+A_{2u}+B_{2u}$
X_5^-	E_g	$A_{1g}+B_{1g}+E_g+E_u$	$A_{1g}+A_{2u}+B_{2u}$
F_{1u}	$A_{2u}+E_u$	$A_{2u}+E_u$	$A_{1u}+E_u$
F_{2g}	$B_{1g}+E_g$	$B_{2g}+E_g$	$B_{2g}+E_g$

such a sequence of phases the associated critical phonon has the symmetry X_2^- and its frequency should vanish when crossing the stability limit line between phases 1, 2, 3 and the phase 0. This is equivalent to write that a_1 varies linearly with temperature and vanishes for $T = T_C$. This stability line coincides with the line of second-order transitions between phase 0 and phases 2 and 3, it coincides with the b_1 axis, and beyond the tricritical point Tr, it lies above the first-order T_d^1-O_h^5 transition line (Fig. 5). Thus for pressure increasing, one follows a parallel to the b_1 axis and there is no possibility for observing a soft mode. Similar arguments are applicable both to the X_4^- OP (since this latter one has the same matrix group) and to the X_5^- OP. This latter OP has an *effective* Landau potential identical to that of the X_2^- OP in equation (4).

Summarizing, we conclude that i) the high-pressure cubic phase is the parent fluorite one, and ii) the direct second-order (or weak first-order) transition from the parent phase to an intermediate tetragonal one is induced by an OP different from X_2^-. The OPs X_1^+ and X_5^+ were discarded as violating the Landau condition. The list of remaining candidates is thus restricted to two OPs that transform the parent phase into only three possible structures: a) the OP X_4^- for $D_{4h}^7(4)$; b) the OP X_5^- for $D_{4h}^{14}(4)$ and c) the OP X_5^- for $D_{4h}^7(4)$ (Tabs. 1, 2).

3.2 Intermediate tetragonal phase

In case a), the X_4^- zone-boundary phonon should become the Raman active B_{1g} mode of the $O_h^5(1) - D_{4h}^{15}(2)$ transformation. However, instead of softening, the corresponding vibration at $\omega = 321$ cm^{-1}, the assignment of which was deduced both by Raman experiments [12,14,26] and lattice-dynamic simulations [19], exhibits an increase of frequency with increasing pressure. Thus the X_5^- phonon remains the only possible candidate involved in the high-pressure phase-transition mechanism. It is worth noting that in this scenario, the soft mode ($\omega = 260$ cm^{-1}) connected to the X_5^- mode is necessarily of E_g symmetry. Since the Raman active vibration at $\omega = 260$ cm^{-1} is of E_g symmetry, the $\omega = 639$ cm^{-1} vibration should be associated with the X_2^- phonon and it acquires A_{1g} symmetry in the D_{4h}^{15} phase.

In order to choose between cases b) and c) let us consider correlations of IRs from the vibrational representation (1) in different phases (Tab. 3). When considering only Raman active components, one can see that the X_2^- mode acquires B_{2g} and E_g symmetry in the D_{4h}^7 and D_{4h}^{14} tetragonal phases, respectively. The closest mode available for interaction with X_2^- is the split F_{2g} mode or, more precisely, its high-frequency component $B_{2g}(\omega = 609$ cm$^{-1})$. So, in the phase D_{4h}^7, one should expect a repulsion (because of the coincidence of symmetry) of these two high-frequency modes with increasing pressure, similar to that observed in the low-frequency range of the Raman spectra (Fig. 3). Experimentally, one observes that the corresponding Raman bands approach each other (see Fig. 3 in [12]). This is in favor of an alternative phase of $D_{4h}^{14}(4)$ symmetry. Simulation of X-ray diffraction from this structure has shown a perfect coincidence of calculated and experimental patterns. This is not surprising as both tetragonal structures are only slightly distorted variants of the parent cubic one. Moreover, since the transformation to the intermediate phase involves only slight distortion of the structure (characterized, for example, by c/a anisotropic ratio), it explains why the characteristic change of the Raman spectra predicted by Table 3 could not be resolved through inevitable line broadening [12]. The magnitude of splitting or the intensity of the new Raman active modes originating from the BZ boundary varies with $(c/a - 1)$ which is close to zero. Thus, a slight peak splitting, for example, is masked by the considerable broadening of the components.

We now summarize the results of our symmetry analysis, starting from the high-pressure fluorite-type structure. The parent phase loses its stability with respect to the X_5^- phonon displacements and undergoes, at $P_2 = 40$ GPa, a second-order phase transition into the tetragonal $D_{4h}^{14}(4)$ phase. Two among the six OP components are non-zero in this phase. From the structural point of view, this means that atomic displacements relating to two of the six eigenvectors of the six-fold degenerated X_5^- phonon will be "frozen" in this phase. The corresponding zirconium

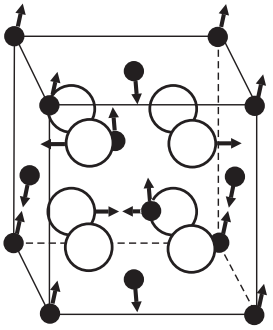

Fig. 6. Atomic displacements associated with the $O_h^5(1) - D_{4h}^{14}(4)$ transition. Small full circles correspond to Zr and large open circles correspond to O atoms.

displacements in the plane perpendicular to a four-fold axis of the tetragonal structure, and oxygens displacements along the four-fold axis are shown in Figure 6. Another phase transition, at $P_1 \simeq 10$ GPa, is induced by the *exchange* of the OPs: X_5^- is replaced by X_2^- and zirconia transforms into the classical tetragonal modification $D_{4h}^{15}(2)$.

3.3 Landau theory of the high-temperature and high-pressure transformations in nano-sized zirconia

The complete investigation of the phase diagram and phase transformations described by two multi-component OPs, X_2^- and X_5^-, is non-trivial. However, the main features can be obtained from a simplified model with two *single-component effective* OPs, taking into account the equilibrium conditions for the X_2^- and X_5^- OP components from Tables 1 and 2. The integrity basis of invariants formed by the X_2^- OP components contains polynomials of second, fourth and sixth degree (see above Eq. (3)) [22,25]. In addition, the corresponding basis for X_5^- also contains eight-degree polynomials [23]. However, direct adjacent of observed tetragonal phases with the parent phase, along with a weak discontinuity observed in experiments, both indicate small OP magnitudes. We therefore restrict the thermodynamic model to the fourth-degree expansion in the OPs $X_5^-(\delta_a)$ and $X_2^-(\delta_b)$:

$$F_1(\delta_a, \delta_b) = a_1\delta_a^2 + a_2\delta_a^4 + b_1\delta_b^2 + b_2\delta_b^4 + g\delta_a^2\delta_b^2. \qquad (5)$$

The lowest degree coupling $g\delta_a^2\delta_b^2$ satisfying the symmetry conditions is included in F_1. The model (5) was first discussed by Lifshitz [27] (see also [22]). The phenomenological coefficients in (5) are assumed to satisfy the conditions $a_2 > 0$, $b_2 > 0$, $g > 2\sqrt{a_2 b_2}$ insuring the positive definiteness of $F_1(\delta_a, \delta_b)$ for large values of δ_a and δ_b. The corresponding equations of state are:

$$\begin{aligned} \delta_a\left(a_1 + 2a_2\delta_a^2 + g\delta_a\delta_b^2\right) &= 0, \\ \delta_b\left(b_1 + 2b_2\delta_b^2 + g\delta_a^2\delta_b\right) &= 0. \end{aligned} \qquad (6)$$

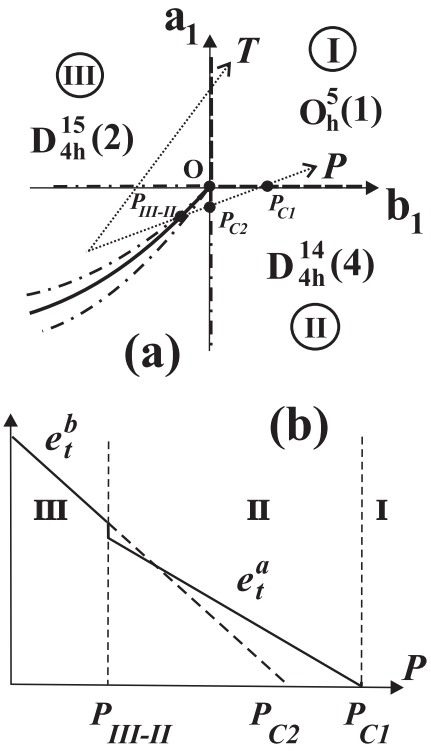

Fig. 7. (a) Cross section of the phase diagram corresponding to a fourth-degree expansion (5) for $\Delta = 4a_2b_2 - g^2 < 0$. Full, dashed, and dash-dotted lines are respectively first-order, second-order, and limit of stability lines. The dotted lines show a possible P-T axis arrangement. (b) Schematic pressure behavior of secondary order parameters.

In addition to the high-symmetry phase I (δ_a=0, δ_b=0), equations (6) describe three low-symmetry phases: II) $\delta_b = -b_1/2b_2$, δ_a=0; III) δ_b=0, $\delta_a = -a_1/2a_2$, and IV) $\delta_a \neq 0$, $\delta_b \neq 0$. In the above case the symmetries of phases are: I - $O_h^5(1)$, II - $D_{4h}^{15}(2)$, III - $D_{4h}^{14}(4)$, IV - $C_{4v}^4(4)$. Figure 7a shows the phase diagram, corresponding to model (5) and satisfying the condition $\Delta = 4a_2b_2 - g^2 < 0$ which insures a direct transition II-III between the tetragonal phases. Assuming the usual linear dependence on temperature and pressure for a_1 and b_1:

$$\begin{aligned} a_1(P,T) &= \alpha_1(T - T_{C1}) + \beta_1(P - P_{C1}), \\ b_1 &= \alpha_2(T - T_{C2}) + \beta_2(P - P_{C2}), \end{aligned} \qquad (7)$$

one can easily describe the phase transformations as follows. The cubic parent phase I transforms into the tetragonal $D_{4h}^{15}(2)$ phase III, by a second-order phase transition under temperature variation. By pressure increase this tetragonal structure transforms into the $D_{4h}^{14}(4)$ phase II, and then into the parent structure. The first pressure-induced transformation is expected to exhibit only a slight discontinuity since this first-order phase transition occurs in the vicinity of the O point (a_1=0, b_1=0) where the OP discontinuity vanishes. The $D_{4h}^{14}(4) - O_h^5(1)$ transition into the parent phase should be continuous (Fig. 7a). Such predictions relating to the thermodynamic character of

transformations evidently correlate with experimental observations. Concerning the phenomenological coefficients in (7) one concludes that α_1 and β_2 are negligible because of a vanishing effect of temperature on X_5^- and pressure on X_2^- observed in experiments.

3.4 Soft mode and secondary order parameters

We now consider the soft-mode behavior, observed for the E_g Raman active band and corresponding to the X_5^- mode in the parent phase. This is an intrinsic feature of our phenomenological model. The connection between the isothermal pressure dependence of an OP and of a phonon frequency follows from the one-dimensional harmonic oscillator equation in linear response [28]:

$$m_{eff}\omega^2 = \frac{\partial^2 F_1}{\partial \delta_a^2} = 2a_1, \tag{8}$$

or, taking into account equation (7),

$$\omega_{sm}^2 = \omega_0^2 \left(P - P_{C1}\right). \tag{9}$$

The latter perfectly fits experimental Raman data (see Sect. 2.3.1, Fig. 3) and one concludes to the existence of a wide pressure range where the linear approximation (7) is valid.

The phase diagram of Figure 7a is entirely determined by the symmetry of the primary transition mechanisms that are proper phonon displacements of the atoms. To describe anomalies in the behavior of macroscopic deformations, observed in XRD experiments, the model of equation (5) should be complemented by taking into account a coupling between the primary OPs and the elastic subsystem. In addition to the primary OP expansion $F_1(T, P, \delta_a, \delta_b)$ (see Eq. (5)), the full variational free energy

$$F(T, P, \delta_a, \delta_b, e_t) = F_1(T, P, \delta_a, \delta_b) + F_2(e_t) + F_3(\delta_a, \delta_b, e_t), \tag{10}$$

contains $F_2(e_t)$, which is a noncritical contribution of the secondary OP, e_t, and the coupling $F_3(\delta_a, \delta_b, e_t)$. For $F_2(e_t)$ we consider, without lost of generality, only uniaxial tetragonal deformations, *i.e.* the single component effective OP $e_t = (2e_{zz} - e_{xx} - e_{yy})$, and restrict the OP expansion to the second degree term:

$$F_2\left(e_t\right) = c_t e_t^2 = \frac{1}{2}\left(c_{11} - c_{12}\right) e_t^2, \tag{11}$$

where c_{11} and c_{12} are cubic stiffness constants. The lowest degree coupling that satisfies the symmetry conditions is included in F:

$$F_3\left(\delta_a, \delta_b, e_t\right) = d_1 \delta_a^2 e_t^a + d_2 \delta_b^2 e_t^b. \tag{12}$$

Here d_1 and d_2 are phenomenological constants. The minimization of F with respect to e_t^i yields, for tetragonal improper deformations, in phases II and III,

$$e_t^a = \frac{d_1}{4c_t \widetilde{a}_2}\beta_1 \left(P - P_{C1}\right), \qquad e_t^b = \frac{d_2}{4c_t \widetilde{b}_2}\beta_2 \left(P - P_{C2}\right). \tag{13}$$

Here $\widetilde{a}_2 = a_2 + d_1^2/4c_t$ and $\widetilde{b}_2 = b_2 + d_2^2/4c_t$ are renormalized phenomenological constants, $P_{C1} > P_{C2}$. Figure 7b shows the corresponding pressure dependences of the secondary OPs and special points.

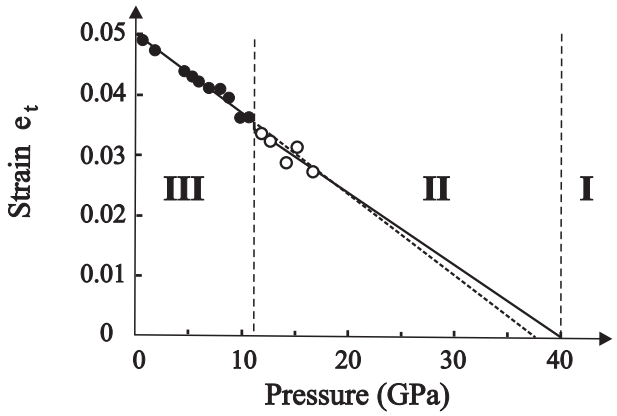

Fig. 8. Spontaneous strains (secondary OPs) e_t^a (open circles) and e_t^b (solid circles) as a function of pressure. Straight lines are the best least-square fits.

Figure 8 presents the theoretically predicted lines (13) fitted to the strains e_t^a and e_t^b calculated from the XRD data. Again, one concludes that despite all restrictions of the phenomenological model (10), it provides an adequate description of the phase transformations in nanosized zirconia.

4 Correlation of vibrational modes in ZrO_2

The present study provides a definitive assignment for the Raman modes in tetragonal ZrO_2. This has been a controversial point (see, *e.g.*, discussion in [26]) especially concerning the position of the A_{1g} soft mode.

The experimental Raman data on **t**-ZrO_2 and **t**-HfO_2 [29] or on stabilized **t**-ZrO_2 with various O^{18} content [30] did not allow the distinction of A_{1g} between the 260 and 639 cm^{-1} modes. Moreover, analysis of stabilized **t**-ZrO_2 have shown that oxygen displacements (which are linked to the A_{1g} mode frequency) can be continuously varied over a wide range of dopant contents [31]. In this spirit, Kim *et al.* have given their preference for a A_{1g} mode at 639 cm^{-1} [32]. This does not agree with the only two available polarized Raman spectra recorded on **t**-HfO_2 by Voron'ko *et al.* [29] and more recently on **t**-ZrO_2 by Merle *et al.* [26]. The latter studies have concluded that the A_{1g} Raman mode should be located at 260 cm^{-1}. However, these results should be considered cautiously as the corresponding A_{1g} mode does not exhibit a clear extinction or even intensity decrease when the polarizer and analyzer are in crossed positions.

Thus, the group-theoretical analysis of the symmetry of the ZrO_2 phases based on reliable XRD and Raman data, resulted in a unequivocal conclusion as to the origin of the Raman active mode $\omega = 260$ cm^{-1} arising from the zone boundary X_5^- phonon. This gives further support to the assignment of the Raman modes at 260 and 639 cm^{-1} to phonons having E_g and A_{1g} symmetry, respectively, in the $D_{4h}^{15}(2)$ tetragonal phase.

5 Conclusions

In summary, the pressure induced phase transitions of nanometric zirconia, ZrO_2, are analyzed *via* a phenomenological Landau approach based on Raman and X-ray diffraction experimental results. The principal conclusion consists in the existence, under high pressure, of a new tetragonal phase $D_{4h}^{14}(4)$ intermediate between the well-known $D_{4h}^{15}(2)$, stable at ambient conditions, and the high-pressure cubic fluorite-type form $O_h^5(1)$. The transformation mechanisms of the pressure-induced phase transitions are identified as displacive. A generalized P-T phase diagram is proposed considering a Landau potential with two OPs having X_2^- and X_5^- symmetry. The soft modes corresponding to the latter are assigned to the $\omega = 639$ cm^{-1} and $\omega = 260$ cm^{-1} Raman modes, respectively.

E. Djurado is acknowledged for the preparation of the sample. We appreciate the kind assistance of M. Mezouar during the high-pressure XRD experiment. We also would like to thank W. Crichton for a critical reading of the manuscript.

References

1. K. Negita, Acta. Metall. **37**, 313 (1989)
2. K. Negita, H. Takao, J. Phys. Chem. Solids **50**, 325 (1989)
3. Y. Ishibashi, V. Dvorak, J. Phys. Soc. Jpn **58**, 4211 (1989)
4. A.P. Mirgorodsky, M.B. Smirnov, P.E. Quintard, T. Merle-Mejean, Phys. Rev. B **52**, 9111 (1995)
5. A.P. Mirgorodsky, M.B. Smirnov, P.E. Quintard, Phys. Rev. B **55**, 19 (1997)
6. M. Wilson, U. Schonberger, M.W. Finnis, Phys. Rev. B **54**, 9147 (1996)
7. K. Parlinski, Z-.Q. Li, Y. Kawazoe, Phys. Rev. Lett. **78**, 4063 (1997)
8. F. Detraux, Ph. Ghosez, X. Gonze, Phys. Rev. Lett. **81**, 3297 (1998)
9. M.W. Finnis, A.T. Paxton, M. Methfessel, M. van Schilfgaarde, Phys. Rev. Lett. **81**, 5149 (1998)
10. S. Fabris, A.T. Paxton, M.W. Finnis, Phys. Rev. B **61**, 6617 (2000)
11. S. Fabris, A.T. Paxton, M.W. Finnis, Phys. Rev. B **63**, 094101 (2001)
12. P. Bouvier, G. Lucazeau, J. Phys. Chem. Solids **61**, 569 (2000)
13. P. Bouvier, E. Djurado, G. Lucazeau, T. Le Bihan, Phys Rev. B **62**, 8731(2000)
14. P. Bouvier, H.C. Gupta, G. Lucazeau, J. Phys. Chem. Solids **62**, 873 (2001)
15. H.K. Mao, J. Xu, P.M. Bell, J. Geophys. Res. **91**, 4673 (1986)
16. A. Hammersley, *ESRF Internal Report, EXP/AH/95-01, FIT2D V5.18 Ref. Manual* (1995)
17. E. Djurado, E. Meunier, J. Solid State Chem. **141**, 191 (1998)
18. E. Djurado, P. Bouvier, G. Lucazeau, J. Solid State Chem. **149**, 399 (2000)
19. A.P. Mirgorodsky, M.B. Smirnov, P.E. Quintard, J. Phys. Chem. Solids **60**, 985 (1999)
20. A.A. Feinberg, C.H. Perry, J. Phys. Chem. Solids **42**, 513 (1981)
21. Yu.M. Gufan, *Structural Phase Transitions* (Nauka, Moscow, 1982), in russian
22. P. Toledano, V. Dmitriev, *Reconstructive Phase Transitions in Crystals and Quasicrystals* (World Scientific, Singapore, 1996)
23. Yu. Gufan, V. Dmitriev, S. Rochal, V. Snezhkov, *Landau Phases in Close Packed Structures* (Rostov Univ. Publ., 1990), in russian
24. A.F. Devonshire, Philos. Mag. **40**, 1040 (1949)
25. Yu.M. Gufan, V.P. Sakhnenko, Soviet Phys. JETP **36**, 1009 (1973)
26. Th. Merle, R. Guinebretiere, A. Mirgorodsky, P. Quintard, Phys. Rev. B **65**, 144302 (2002)
27. E. Lifshitz, Zh. Eksp. Teor. Fiz. **14**, 353 (1944)
28. H. Thomas, K.A. Muller, Phys. Rev. Lett. **21**, 1256 (1968)
29. Y.K. Voron'ko, A.A. Sobol, L.I. Tsymbal, Inorg. Mater. **34**, 350 (1998); Inorg. Mater. **34**, 1098 (1998)
30. B.-K. Kim, S.J. Park, H. Hamaguchi, J. Am. Ceram. Soc. **77**, 2648 (1994)
31. C.J. Howard, B.A. Hunter, D.-J. Kim, J. Am. Ceram. Soc. **81**, 241 (1998)
32. D.-J. Kim, J.-W. Jang, H.-L. Lee, J. Am. Ceram. Soc. **80**, 1453 (1997)